Journal of CO2 Utilization 57 (2022) 101904

Contents lists available at ScienceDirect

Journal of CO2 Utilization

journal homepage: www.elsevier.com/locate/jcou

CO_2 conversion via coupled plasma-electrolysis process

Arunkumar Pandiyan [a,*], Vasileios Kyriakou [a,b], Dragos Neagu [c], Stefan Welzel [a], Adelbert Goede [a], Mauritius C.M. van de Sanden [a,d,**], Mihalis N. Tsampas [a,*]

[a] Dutch Institute for Fundamental Energy Research (DIFFER), 5612 AJ Eindhoven, the Netherlands
[b] Engineering & Technology Institute Groningen, University of Groningen, 9747 AG Groningen, the Netherlands
[c] Department of Chemical and Process Engineering, University of Strathclyde, G1 1XL Glasgow, UK
[d] Department of Applied Physics, Eindhoven University of Technology, Eindhoven 5600 MB, the Netherlands

ARTICLE INFO

Keywords:
CO_2 utilization
Plasmolysis
Electrolysis
SOEC
Oxygen separation

ABSTRACT

Surplus renewable electricity used to convert CO_2 into CO, the building block of liquid fuels, advances the energy transition by enabling large-scale, long-term energy storage and the synthesis of fuel for long-haul transportation. Among the various technologies developed, renewable electricity driven conversion of CO_2 by high-temperature electrolysis and by plasmolysis offer a tantalising potential. High-temperature electrolysis is characterized by high-yield and energy-efficiency and the direct separation of the CO_2 dissociation products CO and O_2. However, the difficulty to break the carbon-oxygen double bond poses challenging requirements on electrode materials. CO_2 plasmolysis on the other hand, offers a similar energy efficiency, does not employ scarce materials, is easy to upscale, but requires efficient gas separation and recuperation because the produced CO remains mixed with O_2 and residual CO_2. Here, we demonstrate that the coupling of the two processes leads to a renewable-electricity-driven route for producing CO from CO_2, overcoming the main bottleneck of CO_2 plasmolysis. A simulated CO_2 plasmolysis gas mixture is supplied to a high-temperature electrolyser to separate the product gases electrochemically. Our results show that the product stream of the coupled-process contains 91% less oxygen and 138% more CO compared with the bare plasmolysis process. Apart from upgrading the produced gas mixture, this coupled approach benefits from material stability. Durability tests (~100 h) show better stability in coupled operation when compared with conventional CO_2 electrolysis. Synergy between plasmolysis and electrolysis opens up a novel route to efficient CO_2 conversion into valuable CO feedstock for the synthesis of long-chain hydrocarbons.

1. Introduction

The energy transition is a necessary response to climate change, caused by the increased concentration of greenhouse gases (GHG) in the Earth atmosphere, the result of anthropogenic GHG emissions, CO_2 being the main contributor [1]. The 2015 UN-FCCC pledges to limit the temperature rise of the Earth surface to 2 °C in order to mitigate its adverse effects on environment and society, and to call for an investigation to limit to 1.5 °C. With a global average temperature rise of 1.0 °C above pre-industrial level already reached to date, this target becomes increasingly elusive [2]. Hence, the energy transition needs to be accelerated in order to reach a sustainable energy system by the middle of this century.

Some sectors of the energy system are less amenable to sustainable solutions than others, in particular chemical industry and long-haul transportation prove challenging. Integration of current renewable energy technology, mainly solar and wind generated electricity, runs into some fundamental limitations [3–5], including its intermittent nature requiring large-scale, long term energy storage and the fact that these sectors require high temperature heat or high energy density fuels. Thus, the urgent need arises for the development of technologies converting renewable electric power into storable chemical fuels, the Power-to-X (P2X) technology.

Carbon dioxide (CO_2) is a key molecule in P2X technology [4–8]. The dissociation of CO_2 to CO and O_2 is a strongly endothermic process. Sustainable production of CO would be a means to implement renewable energy into the chemical production chain whilst adding value to the CO_2 emitted [9,10]. Central is the production of syngas, a mixture of CO

* Corresponding authors.
** Corresponding author at: Dutch Institute for Fundamental Energy Research (DIFFER), 5612 AJ Eindhoven, the Netherlands.
E-mail addresses: a.pandiyan@differ.nl (A. Pandiyan), m.c.m.vandesanden@differ.nl (M.C.M. van de Sanden), m.tsampas@differ.nl (M.N. Tsampas).

https://doi.org/10.1016/j.jcou.2022.101904
Received 9 November 2021; Received in revised form 16 January 2022; Accepted 19 January 2022
Available online 25 January 2022

and H_2, the latter obtained via the CO to water gas shift reaction, from which liquid fuels are synthesised via the Fischer-Tropsch process [11]. Research on CO_2 to CO conversion is based on electrochemical [12,13], solar thermochemical [14,15], photoelectrochemical [16,17] and photochemical [18,19] approaches as well all their possible combinations. In recent years, there has been an increasing interest in the use of plasma technology for CO_2 conversion [20–47].

In non-thermal plasmas (i.e. the electrons have a much higher temperature than then gas) energetic electrons can be used for gas activation, and thermodynamically unfavored reactions, such as CO_2 splitting (or plasmolysis, see Eq. 1), can occur at a reasonable energy cost [8,36–39]. In thermal plasmas efficient gas heating can be realized leading to thermal dissociation of the gas injected [8,23,24,41]. CO_2 plasmolysis has been demonstrated in different types of non-thermal plasmas and configurations, e.g. microwave (MW) [21–25], Dielectric Barrier Discharge (DBD) [26–28], DC glow discharge [29], Gliding Arc (GA) [30–33] and Radio Frequency (RF) [34]. However, the (close to) thermal MW and GA discharges are considered reported to be the most promising plasma systems for CO_2 decomposition due to their capability to utilize the highly efficient vibrational excitation kinetics of the non-equilibrium discharge. For CO_2 plasmolysis under nonthermal conditions using these discharge, energy efficiencies of up to 80% have been reported [8,35–41].

$$CO_2 \xrightarrow{Plamolysis} CO + \frac{1}{2}O_2, \quad \Delta H = 2.9\text{eV} \Big/ CO_2 \tag{1}$$

Plasma technology does not rely on scarce materials and provides fast switching characteristics (on/off) with high power density and easy upscaling. The main challenge for developing this technology is how to get efficient CO_2 conversion with high energy efficiency and how to prove its feasibility on an industrial scale. There is plethora of research focused on modeling, reactor optimization and incorporation of catalysts in order to improve simultaneously conversion and energy efficiency [41–47]. Nevertheless, there is another important bottleneck of CO_2 plasmolysis, which hinders its practical implementation, is that the product stream contains a mixture of CO, O_2, and unreacted CO_2 (Fig. 1a) [8,35–39,48,49]. Due to the presence of O_2, this mixture has a low chemical feedstock value because the conventional chemical processes [11] will enable the back reaction (i.e., CO oxidation to CO_2). It is therefore of critical importance to separate the O_2 from the product stream. Physical separation of oxygen from this gas mixture is very challenging and it is difficult to achieve stable CO_2 resistance electrode materials and membranes [48,49]. In this work, and aiming for a renewable energy driven process we examine the use of solid oxide electrolysis cells (SOECs) for valorising the plasmolysis product stream (Fig. 1a). The suggested coupling of plasma and SOEC is in principle applicable for all types of plasmas, however, as study case here we have selected MW plasmas, which is validated from the high reported energy efficiencies and our expertise in the field [23–25,41].

SOECs are primarily known as a promising pathway for H_2O and/or CO_2 electrolysis [13,50–52] but can also be employed for electrochemical oxygen separation from oxygen-containing gas mixtures [53–56]. Depending on system design and operating conditions, the electric energy consumption for SOEC oxygen separation can be made comparable with cryogenic air separation and is significantly lower than pressure swing adsorption [56]. SOECs operate in the temperature range of 600–900 °C and utilize a ceramic electrolyte with O^{2-} conductivity. As in any electrochemical cell, two electrodes are deposited on each side of the electrolyte; in case of CO_2 electrolysis, CO is produced at the fuel electrode (cathode) and O_2 at the oxygen electrode (anode) [13,57]. Although SOEC technology offers high efficiencies, its high operating temperature causes durability problems related to electrode materials degradation. This degradation is related to various factors, including electrode structural integrity, delamination, and poisoning of active site. More durable SOEC electrode materials for CO_2 electrolysis is typically found in strategically synthesized perovskite-type oxides [13,50–52,57,58].

Perovskite-type oxides (ABO_3) are among the most promising electrode materials for conventional CO_2 electrolysis. Perovskites exhibit mixed ionic electronic conductivity as single phases and can accommodate several kinds of defects under redox conditions, allowing them to adapt to various external conditions and maintain stability and

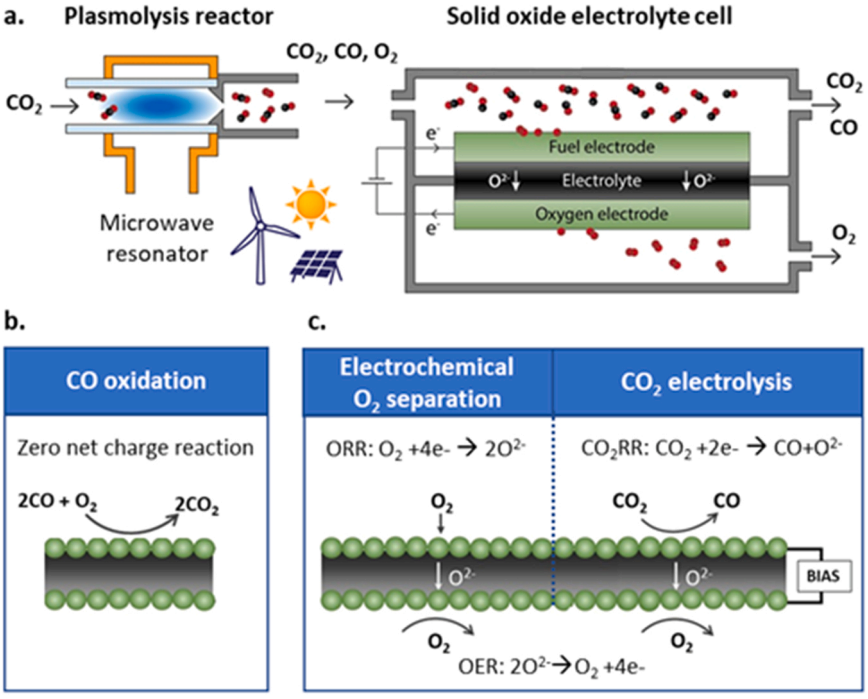

Fig. 1. (a) Concept of plasma-electrolysis for CO_2 valorisation via MW plasmolysis and SOEC oxygen separation. Schematic illustration of the plasmolysis reactor coupled SOEC configuration (b) zero net charge reaction and (c) electrocatalytic SOEC reactions (OER stands for oxygen evolution reaction, ORR for Oxygen Reduction Reaction, CO_2RR for carbon dioxide reduction reaction).

functionality under redox environment [13,57–69]. An important advantage of perovskites is that they can be used as fuel and as oxygen electrodes in symmetrical configuration, thus decreasing the overall cell preparation cost and complexity [59,60]. To date, $Sr_2Fe_{1.5}Mo_{0.5}O_{6-\delta}$ (SFM), $(La_{0.75}Sr_{0.25})_{0.97}Cr_{0.5}Mn_{0.5}O_{3-\delta}$ (LSCM), $La_{0.8}Sr_{0.2}FeO_{3-\delta}$ (LSF) and $La_xSr_{1-x}TiO_{3-\delta}$ (LST) based electrodes have shown the most promising results [61–65]. In this work, SFM-based electrodes have been selected for their wide operating temperature range (650–850 °C) essential for this investigation [66–68].

In this contribution, we examine the in series coupled operation of MW plasma reactor and SOEC, where the CO_2 plasmolysis product stream (composed of CO_2, CO, and O_2) is fed into the SOEC, aiming to valorise the overall product stream (Fig. 1a). In this configuration, three reactions can occur at the fuel electrode (Fig. 1b and c); (i) catalytic CO oxidation, (ii) oxygen reduction reaction (ORR), and (iii) carbon dioxide reduction reaction (CO_2RR). CO oxidation on the fuel electrode is an undesired reaction because it reduces valuable CO output, and thus, it must be suppressed. This can be achieved either by lowering the operating temperature and/or by accelerating the kinetics of the ORR and CO_2RR. Furthermore, as in conventional CO_2 electrolysis, the fuel electrode should possess chemical and structural stability under CO_2 gas exposure and with reducing potentials applied. We demonstrate that SOEC operation with a CO_2 plasmolysis product stream at the fuel electrode not only separates oxygen efficiently but also improves the SOEC durability compared with conventional dry CO_2 electrolysis.

2. Results and discussion

2.1. Expected reactions and processes during coupled plasma-electrolysis process

The evaluation of SOECs for oxygen separation under a CO_2 plasmolysis equivalent gas mixture is a rather complex process, involving three reactions, i.e., CO oxidation, ORR, and CO_2RR (Fig. 1b,c). At the fuel electrode surface, the catalytic oxidation of CO to CO_2 (zero net charge reaction) may occur, either at OCV or under imposed bias. This is an undesired reaction since it decreases the valuable CO flux. Upon imposing negative bias, two electrochemical reactions may take place at the fuel electrode: ORR: $O_2 + 4e^- \rightarrow 2\,O^{2-}$ and CO_2RR: $CO_2 + 2e^- \rightarrow CO + O^{2-}$ (Fig. 1c). Both these reactions result in the oxygen evolution reaction (OER) at the oxygen electrode. Furthermore, via ORR, the undesired CO oxidation can be hindered by decreasing oxygen availability. Via CO_2RR, the residual CO_2 from the plasmolysis gas mixture is electrochemically reduced into CO, thereby increasing the CO yield.

The reaction pathways considerably depend on the applied voltage and the operating temperature. According to thermodynamics, the reversible potential for driving CO_2 electrolysis (i.e., CO_2RR and OER) varies from 0.95 V to 0.81 V ($\Delta G = 185$ KJ/mol to 156 KJ/mol), within the temperature range of 650–850 °C (Fig. S1). On the other hand, electrochemical oxygen separation (i.e., ORR and OER) occurs at all applied bias voltages since it concerns a process with similar initial and final points (i.e., the Gibbs free energy for the electrochemical oxygen separation is zero). Nonetheless, kinetically the system is not ideal, displaying polarization or activation losses, thus an overpotential is always required to drive the O^{2-} across the SOEC.

2.2. SOEC materials and microstructure

To explore the individual reaction schemes described above, symmetrical SOECs were fabricated, with both the fuel and oxygen electrodes composed of SFM-GDC (Fig. S2) deposited on ScCeSZ electrolyte. Fig. 2a-c displays the surface and cross-sectional microstructure of the SOEC. The SFM-GDC electrode thickness was ~15 μm and with relatively high open porosity to facilitate the diffusion of gases into the electrode-electrolyte interface. A GDC buffer layer was utilized to improve the adhesion of SFM-GDC to the ceramic electrolyte, as well as to prevent the reaction of Sr with Zr at the electrode-electrolyte interface (Fig. 2a) [23,24,60,69].

2.3. Testing conditions and plasmolysis equivalent gas mixture

Following fabrication, the cells were fitted into an in-house testing facility for the electrochemical oxygen separation studies. The experiments were carried out at temperatures between 650 °C and 850 °C. To simulate the effluent of a plasma reactor, a CO_2 plasmolysis equivalent gas mixture of 7% CO_2, 3% CO and 1.5% O_2 diluted in He was employed. The composition of this gas mixture was selected based on two criteria (i) to simulate a 30% conversion of the CO_2 plasmolysis that is typically obtained in our MW plasma reactors in a wide pressure range [23–25, 41] and (ii) to match the oxygen separation potential of our SOEC with the detection sensitivity of our diagnostics. To further elaborate on this our SOEC setup [46–48] (Fig. S3) can accommodate samples with active electrode area < 1 cm^2 which means that with state of the art current densities (~1 A/cm^2) we can only separate oxygen < 4 sccm. Thus dilution in He was selected in order to allow us to follow changes in the gas composition upon electrochemical oxygen separation. The total volumetric flowrate was 60 sccm in the fuel electrode compartment, whereas 30 sccm of air was fed to the oxygen electrode side to purge the

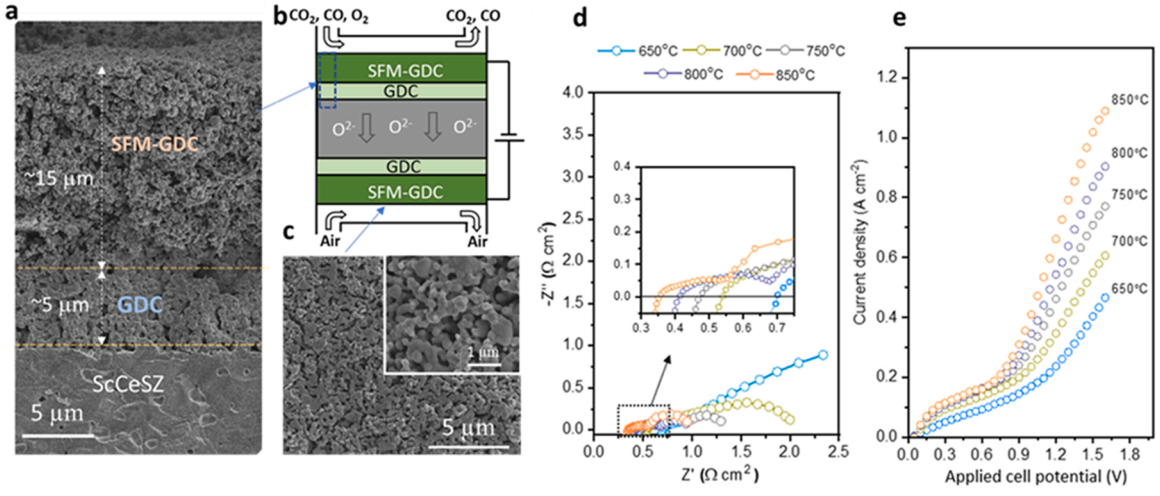

Fig. 2. (a-c) SEM image of as-sintered surface morphology and cross-section of the fabricated cell at the position indicated in the SOEC schematic. Electrochemical performance of SFM-GDC under plasmolysis gas composition (CO_2/CO/O_2) in SOEC mode at different operating temperature (e) Nyquist Plot (f) IV curve.

electrochemically pumped oxygen.

2.4. Performance evaluation under coupled plasma-electrolysis

Electrochemical impedance spectroscopy (EIS) has been performed to analyse the resistance of the developed cell (Fig. 2e). The Nyquist plots from EIS at OCV conditions revealed two arcs. The high-frequency intercept with the x-axis (Z′ real) represents the cell's ohmic resistance, which is mainly determined by the electrolyte. The difference between low- and high- frequency intercepts represent the cell's polarization resistance (Rp). Increase in operating temperature significantly decreases both ohmic- and polarization- resistances. Specifically, at 650 °C, the observed Rp is 4.1 times higher (3.55 Ω cm^2) than 850 °C (0.85 Ω cm^2), indicating that the SOEC processes taking place are thermally activated. Subsequently, SOEC cell performance was evaluated by using the characteristic I-V curves at different temperatures (Fig. 2f). The current density at 1.5 V was found to increase from 0.43 A·cm^{-2} at 650 °C to 1.0 A·cm^{-2} at 850 °C. By taking into account the relatively high solid electrolyte thickness of ~150 μm, the obtained current densities are close to what is expected from state-of-the-art SFM based SOECs [59,64,66,67]. Furthermore, these results support the suitability of SFM-GDC electrode material since these high currents correspond to high oxygen transport through the solid electrolyte, which is essential for the success of the proposed concept.

2.5. Oxygen separation and carbon dioxide splitting capabilities

In order to evaluate the coupled plasma-electrolysis process, we performed transient potentiostatic experiments with product analysis of the fuel electrode effluent by means of gas chromatography (GC) and by infra-red (IR) analysis. The discrimination of the electrochemical O_2 separation and CO_2 electrolysis was done by following the levels of CO_2, CO and O_2 with our diagnostics, before and after current applications. By using mass balance calculations and Faraday's law it is possible to deconvolute between O_2 electrochemical separation and CO_2 electrolysis. Fig. 3a depicts the current density and the corresponding oxygen flux obtained through the electrolyte during such experiments, consisting of a sequence of 20 min duration voltage steps ranging from 0.25 V to 1.5 V in 0.25 V steps. The current density was stable during the imposed voltages up to 1.0 V, while at voltages above 1.0 V, it slightly tails off during the first few minutes until a steady-state is reached.

Fig. 3b displays the rate of oxygen separation (ORR and OER) from the CO_2/CO/O_2 plasmolysis composition (Fig. 2b). The O_2 removed from the mixture follows a linear trend in all cases, reaching up to 0.50 and 0.71 ml min^{-1} cm^{-2} at 650 °C and 850 °C, respectively, at 1.5 V cell voltage. On the other hand, CO_2 electrolysis occurs at potentials ≥ 1.0 V at all tested temperatures due to the significant energy required for cleaving the CO_2 molecule (Fig. 1b and S2). In Fig. 3c, the experimentally observed voltage zone for CO_2 electrolysis was between 1.0 V and 1.5 V with the oxygen flux ascribed to this reaction corresponding up to 0.6 at 650 °C and 1.6 ml min^{-1} cm^{-2} at 850 °C, respectively. The overall Faradaic efficiency exceeds 92% under all applied voltages and operating temperatures, with a relative error of 5% (Fig. 3d), exhibiting the high selectivity of SFM-GDC oxygen separation and CO_2 electrolysis.

To better understand the possible scenarios for oxygen separation, the relative levels of CO and O_2 versus their inlet (feed) rate, were calculated from the corresponding mass balances during the transient experiments. Fig. 3e and 3f shows CO and O_2 level which clearly exemplify the selectivity of O_2 separation either from molecular O_2 or CO_2 electrolysis of CO_2/CO/O_2 by varying the applied voltage and as function of operating temperature. For instance, by imposing a voltage which is lower than the onset potential for splitting CO_2 (i.e., ≤ 0.75 V), the electrochemical O_2 flux originates only from the available molecular O_2 in the plasmolysis mixture. When the applied potential exceeds the onset potential for CO_2 electrolysis (i.e., ≥ 1.0 V), then the CO_2 electrolysis scheme also contributes to the oxygen transport through the

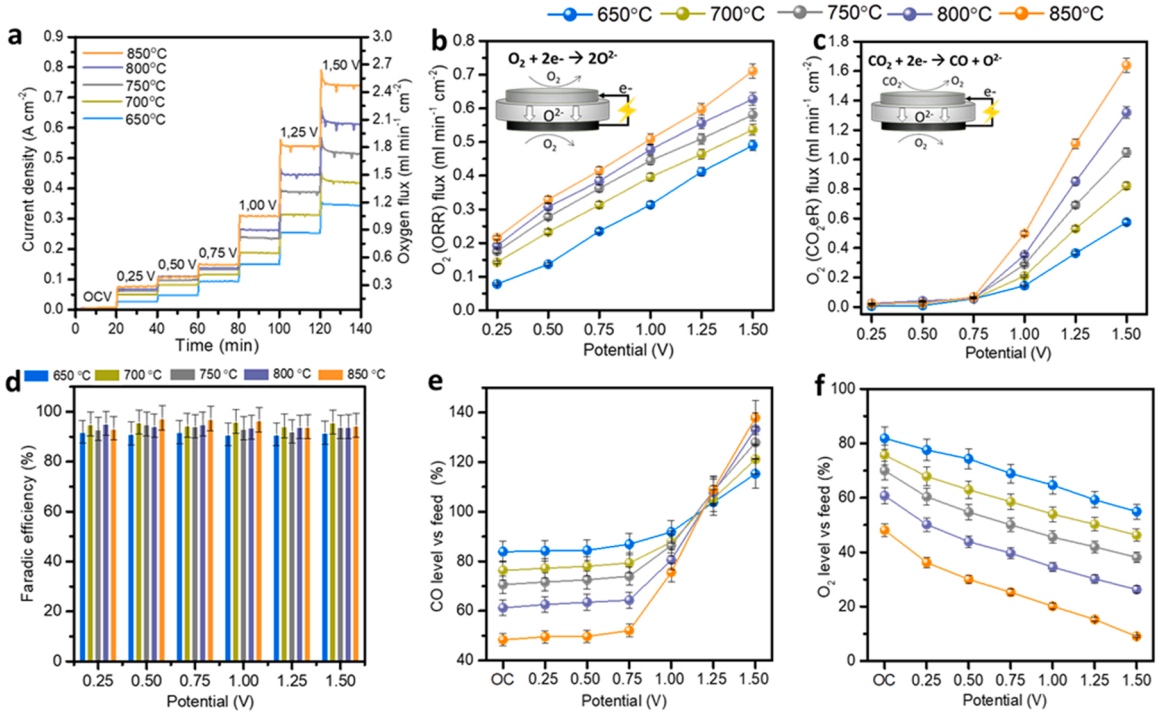

Fig. 3. (a) Potentiostatic transient experiments: Effect of time on current density at the different applied voltages of 0.25, 0.50, 0.75, 1.00, 1.25, and 1.50 V, respectively. Oxygen recovery rate from CO_2/CO/O_2 mixture due to (b) the direct O_2 removal (ORR) and (c) CO_2 reduction (CO_2RR), as a function of the applied voltage. (d) Faradaic efficiency of the O_2 recovery process. (e) CO and (f) O_2 levels at the exit of the cathode compartment with respect to the inlet plasmolysis CO_2/CO/O_2 gas composition at different operating temperature, where the region below ≤ 0.75 V the electrochemical O_2 flux originates only from the available molecular O_2 and above ≥ 1.0 V the O_2 flux originate from both O_2 and CO_2 electrolysis. Feed in fuel electrode: 7% CO_2, 3% CO and 1.5% O_2 diluted in He, 60 sccm flow rate.

solid electrolyte. Interestingly, at such operating conditions, the SOEC not only separates oxygen from the plasmolysis effluent mixture electrochemically but also valorises this mixture by enriching it with CO. This is illustrated in Fig. 3e through the measured CO values exceeding 100% vs the inlet feed. At the same time, the O_2 ratio decreases linearly down to ~9% at 1.5 V and 850 °C (Fig. 3f). The CO losses (Fig. 3e) are decreased when lowering the operating temperature however this is a challenge that needs to be addressed in the future by investigating alternative electrode materials with lower catalytic activity for CO oxidation.

As discussed above, only 52% of the supplied CO flux had remained under OCV at 850 °C due to its oxidation, thus significantly decreasing the CO value of the plasmolysis exit stream. Upon applying potentials up to 0.75 V, the electrochemically separated oxygen is exclusively obtained from ORR, without affecting the CO levels which were already degraded due to CO oxidation. Now, by imposing a voltage ≥ 1.0 V, CO concentration go up to 138% when compared with CO input levels at 850 °C as a result of CO production by CO_2RR. Therefore, these results show that the application of low potentials (≤ 0.75 V) can selectively remove oxygen from the $CO_2/CO/O_2$ gas stream, while at high potentials (≥ 1.0 V), both CO_2RR and ORR occurs at the fuel electrode, resulting in the simultaneous oxygen separation and mixture upgrading via electrocatalytic reduction of residual CO_2.

2.6. Comparison with the conventional dry CO_2 electrolysis

In this section, SOEC operation with a plasmolysis gas mixture was benchmarked against the conventional dry CO_2 electrolysis process [12, 13]. The SOEC cell configuration used in the CO_2 electrolysis process was identical to the one used for the electrochemical oxygen separation from the plasmolysis gas mixture. During conventional dry CO_2 SOEC electrolysis, the fuel electrode is supplied with 10% CO_2 mixed in He in order to match the total CO_2 rate in both plasmolysis-SOEC and dry CO_2 electrolysis approaches.

Fig. 4a-c show the I-V polarization curves obtained at the different temperatures examined. As expected, at applied potentials below 1.0 V, where the CO_2RR is thermodynamically limited, the current density during conventional operation is practically negligible. By introducing the plasmolysis mixture, however, current densities up to 0.21 A cm^{-2} at 850 °C were attained, which correspond to ~0.71 ml min^{-1} cm^{-2} of electrochemically separated oxygen from the gas mixture to the oxygen electrode. At potentials ≥ 1.0 V, the imposed potential exceeds the thermodynamic threshold and CO_2RR proceeds with an identical rate with the plasmolysis SOEC coupled approach. This observation is clearly demonstrated at 750 °C and 850 °C in when the current densities become practically identical. The effect of polarization on the rate of CO production is shown in Fig. 4d-f. With the equivalent CO_2 plasmolysis composition, the total CO yield reached up to 2.0 ml·min^{-1}·cm^{-2} at 1.25 V and 850 °C whilst under the same conditions, the CO_2 electrolysis system results in lower CO production rate of 1.45 ml·min·cm^{-2}.

The benefit of employing the coupled plasmolysis SOEC approach for CO recovery becomes more pronounced by decreasing the operating temperature, where the CO rate exiting the fuel electrode compartment is more than double the amount of CO produced from CO_2 electrolysis. More specifically, at 1.25 V, the CO production rate is 2.0 ml·min·cm^{-2} at 750 °C and 1.90 ml·min·cm^{-2}at 650 °C for the plasmolysis condition, whereas for electrolysis this is more than halved to 0.91 ml·min^{-1}·cm^{-2} at 750 °C and 0.62 ml·min·cm^{-2} at 650 °C.

2.7. Durability of the SOEC cells

In the evaluation of SOEC performance it is of critical importance to assess its long-term stability and identify the primary reasons for degradation. In our assessment, we applied a voltage of 1.25 V at 750 °C for 100 h by exposing the SFM-GDC electrode to both CO_2 (for evaluating CO_2 electrolysis) and $CO_2/CO/O_2$ (for evaluating the coupled operation). In case of CO_2 electrolysis at 1.25 V, Fig. 5a reveals considerable degradation rate of ~0.65 mA·h^{-1}, with the current density decreasing from 375 to 310 mA cm^{-2}, over the 100 h of testing (17% performance loss). On the other hand, the cell operated under plasmolysis gas mixture displayed a modest degradation rate of ~0.29 mA·h^{-1} leading to a total current loss of ~5%. To explore the coupled process

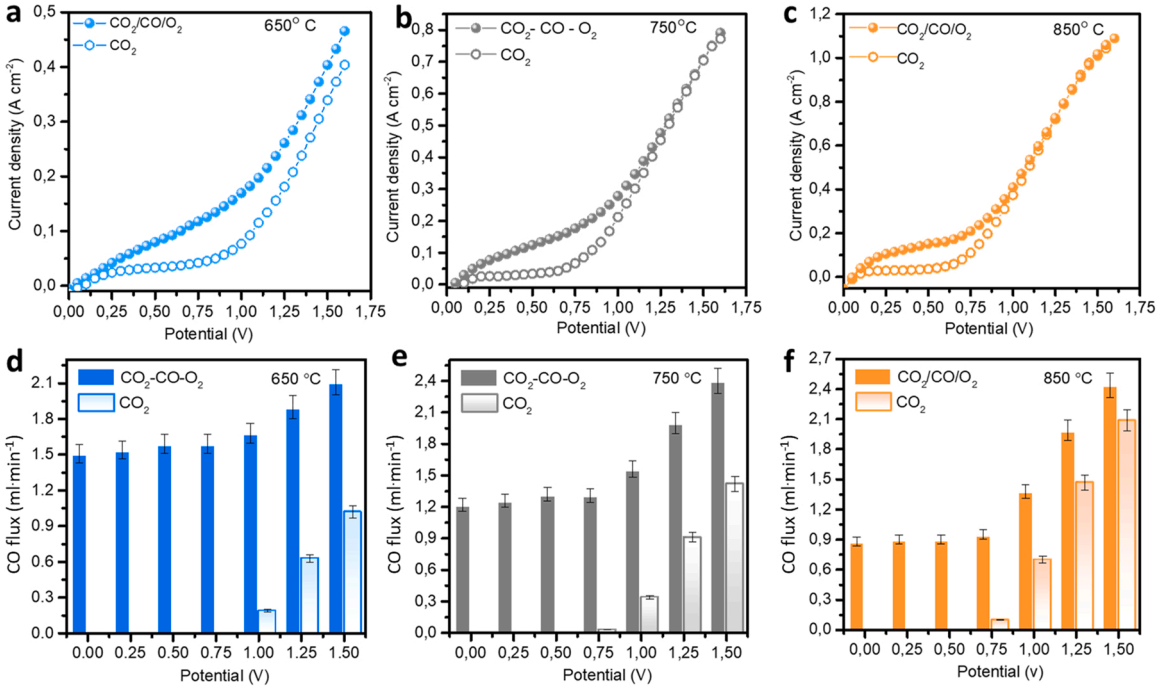

Fig. 4. Dependence of current densities (a)-(c) and the corresponding CO recovery rates (e)-(f) on cell voltage for a plasmolysis gas mixture against conventional CO_2 electrolysis at temperatures (a), (d) 650 °C (b), (e) 750 °C (c), (f) 850 °C. Feed in fuel electrode: 7% CO_2, 3% CO and 1.5% O_2 diluted in He, for CO_2 plasmolysis equivalent gas mixture and 10% CO_2 diluted in He for conventional CO_2 electrolysis, 60 sccm flow rate.

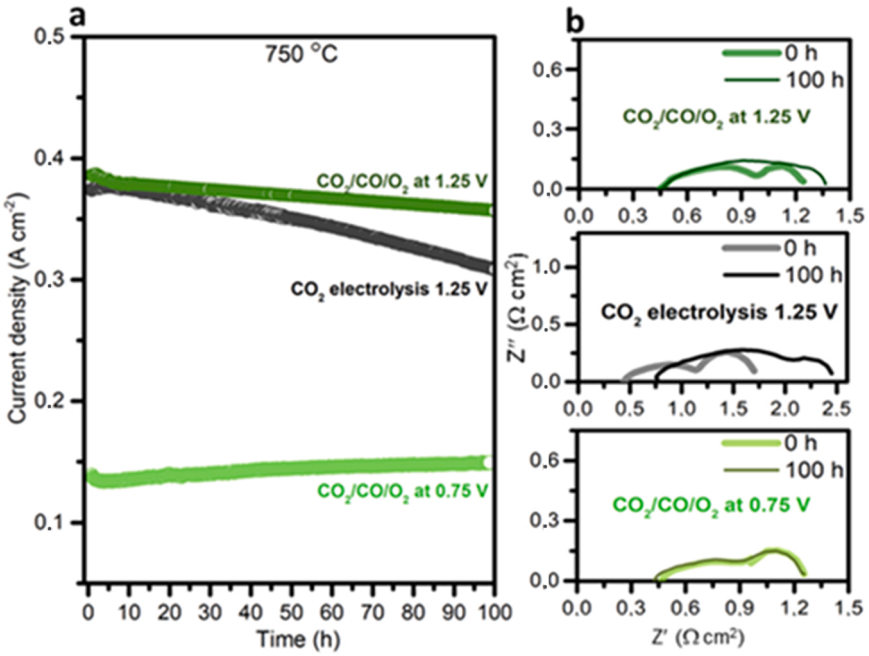

Fig. 5. (a) Durability test of SFM-GDC fuel electrode at constant applied voltage under plasmolysis composition (at 0.75 V and 1.25 V) and CO_2 electrolysis (at 1.25 V). (b) Electrochemical impedance spectroscopy of SOEC (at OCV) before and after 100 h of operation under plasmolysis composition and CO_2 electrolysis at 750 °C.

at conditions where CO_2RR is not feasible, we performed a stability test at 0.75 V.

In contrast, the performance during the coupled operation at 0.75 V (i.e. slightly milder reducing voltage treatment) was "activated" over the time since the current density increased by 7%. According to the EIS results (Fig. 5b), the cell total resistance presented a small drop from 0.42 to 0.47 Ω cm^2 within the initial 100 h. However, the polarization resistances of SOEC remain almost the same during the durability test (0.81 Ω cm^2 at the beginning of the experiment and 0.80 Ω cm^2 at the end). We hypothesize that the activation might be associated with the reorganization of fuel electrode microstructure and/or interface with current collection [70,71].

The Nyquist plot from EIS analysis was employed to provide indications as to the electrochemical origins of the observed degradation at 1.25 V. In the case of plasmolysis gas mixture, only minor changes in polarization resistances, by 7% increase, were detected. During the

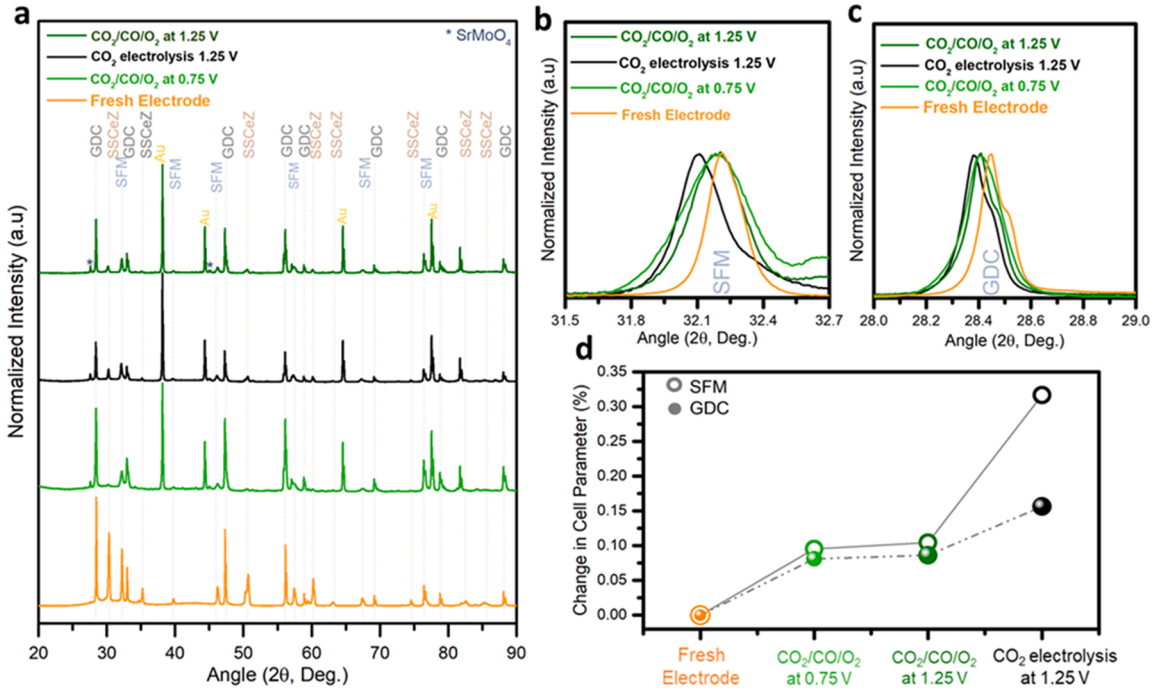

Fig. 6. (a) XRD patterns of SFM-GDC sample before (fresh) and after durability test at constant applied voltage under plasmolysis composition (at 0.75 V & 1.25 V) and CO2 electrolysis (at 1.25 V). (b) Focus on (110) SFM peak (c) Focus on (111) GDC peak (d) Change in cell parameter (%) with respect to fresh electrode at the various operating conditions after durability test.

conventional CO_2 electrolysis, both ohmic and polarization resistances increased compared to the fresh sample by 47% and 27%, respectively (Fig. 5b). Therefore, the change in ohmic and polarization resistance, indicating possible degradation of the contact and thus interface between cell components (i.e. electrodes and electrolyte), but also possible degradation of the electrode capacity to catalyse electrode reactions. This points towards microstructural and compositional changes at the SFM-GDC interface as well as at the surface of the electrodes. However, by performing SEM analysis of the sample, no visible change was observed (Fig. S4 and S5).

Since we did not observe interpretable differences from SEM, we examined the changes in the average structure of the materials across these different operation scenarios. The XRD pattern and change in cell parameter are summarized in Fig. 6 and Fig. S6 It can be seen that SFM-GDC maintains the phase structure in both CO_2 electrolysis and plasmolysis condition as it was in the fresh, with an extra weak reflection from the $SrMoO_4$ secondary phase. Previous research revealed that this co-existence of minor secondary peaks in SFM solid solution has negligible effect on the electrode performance [66,72,73].

These results indicate that as compared to the fresh electrodes, the CO_2 electrolysis mode imposes the most dramatic changes in lattice parameters following operations. For the SFM phase this is 0.31% and for the GDC this is 0.15%. Clearly, SFM exhibits significantly more lattice expansion under operation as compared to GDC, which will likely lead to delamination of the two phases. Indeed, the difference in expansion observed for these phases, x-y, is consistent with a threshold for delamination issues observed for mismatch in thermal expansion coefficients or chemical expansion mismatch [74,75]. Since SFM electronic conductivity is much higher than ionic one [76,77] the role of GDC is to provide oxide ions for the reaction, the active region in the electrode is the interface between GDC and SMF and any delamination between them will translate into degradation of both ohmic and polarisation resistance, which is consistent with the observed degradation.

In order to accelerate these degradation mechanisms, and provide additional evidence of the above conclusion, between SFM and GDC, we removed from the fuel electrode GDC and carried out the same experiments in both plasmolysis gas mixture and dry CO_2 electrolysis with the same oxygen electrode, i.e., SFM-GDC (Fig. S7). The new SOEC configuration was SFM/GDC/ScCeSZ/GDC/SFM-GDC. After 100 h of operation, clear delamination was observed at the SFM electrode interface and GDC buffer layer for CO_2 electrolysis (Fig. S8). This microstructural damage in the absence of GDC under CO_2 electrolysis conditions rapidly deteriorates the cell performance by 1.73 $mA{\cdot}h^{-1}$, which is ~2.7 times faster than the composite electrode (Fig. S9 vs Fig. 5). By contrast, when conditions were changed to the plasmolysis gas mixture, no evidence of delamination at the SFM and GDC interface was observed (Fig. S8, S9). In particular, the performance of SFM under plasmolysis gas condition at 1.25 V exhibited a degradation rate of 0.25 $mA{\cdot}h^{-1}$, whereas, at 0.75 V, the cell performance was improved (by 5%) during the 100 h. These results are in agreement with measurements utilizing the composite SFM-GDC electrode.

2.8. Physicochemical characterization of electrode materials

The above results clearly show that the fuel electrode operated under conventional CO_2 electrolysis conditions undergoes severe microstructural changes, resulting in delamination and performance loss. To further understand these changes, an in-depth analysis by XPS and XRD (Fig. 6, S6, S10, S11) was carried out to the fresh and used (100 h stability) samples presented in the supplementary section. The main outcome of the combined XPS and XRD analysis of the fuel electrodes is that operation under plasmolysis gas mixture has a marginal effect on lattice expansion compared to the major modifications identified under dry CO_2 electrolysis.

Our analysis suggests that the continuously applied, high cathodic voltage decreases the valence of the Mo, Fe, and Ce, leading to lattice expansion, which could be the source of the delamination at the SFM and GDC interface (Table S1-S2). This phenomenon was not observed when the fuel electrode were exposed to the plasmolysis gas mixture. We attributed this effect to the presence of molecular oxygen (O_2) in the plasmolysis gas mixture (CO_2/CO/O_2), which is beneficial for the SFM perovskite in order to retain the valence state of the Mo, Fe, and Ce ions in SFM-GDC, and thus to lower the lattice expansion in order to diminish delamination during long-term operation. Therefore, this coupled CO_2 plasmolysis and SOEC approach not only maximises the CO yield through the CO_2RR pathway but also improves the chemical integrity of the cell compared with the traditional dry CO_2 electrolysis approach.

2.9. Energy consumption considerations

CO_2 plasmolysis reactors are reported to operate up to 80% energy efficiency, which is similar to values reported for CO_2 electrolysis [8,39,40,52,57,76]. However, the energy stored in the product stream of plasmolysis, without the step of oxygen separation, can be used only for heating purposes (i.e. via CO oxidation). If only pure CO is needed as feedstock for chemical plants then oxygen separation is essential [11]. Thus it is interesting to define and evaluate the energy consumption for decoupling CO molecules from their O_2 counterparts (from the CO_2 dissociation, Eq. 1). In order to do this we should focus on the region that only oxygen separation is taking place i.e. operating voltage < 0.75 V.

In the current study the energy needed for making a CO molecule oxygen unpaired (at the conditions of Fig. 5) account to 56.5% of the CO energy content (see SI). Thus the energy efficiency of CO production (after oxygen separation) via the coupled operation (as described in Fig. 1) should be the product of 56.5% and the efficiency of plasmolysis alone. As a figure of merit if one considers CO_2 plasmolysis in the range of 60–80% energy efficiency then in the coupled operation the overall energy efficiency will be 34–45%. This however should not be considered as the best performance that can be obtained. The reason is that the energy spent for oxygen separation process is mainly for overcoming kinetic limitations. By implementing advanced SOEC architectures (with thinner electrolyte and/or supporting electrode) [78–84] ohmic losses can be further reduced and thus, the electrical energy consumption for the oxygen separation can be decreased. In such SOEC the operating temperature can be further decreased ($< 600\ ^{o}C$) and in combination with electrode materials with lower CO oxidation activity than SFM it is expected to mitigate the CO losses challenge, while at the same time better OER electrodes could be used to improve the current densities.

Our durability studies in combination with the previous analysis suggest that one can envision an integrated (renewable) electrically-driven plasma-electrolysis approach (i.e. where plasmolysis and SOEC are composing a single system in which heat losses from plasmolysis reactor are used to heat the SOEC) could be competitive with the CO_2 electrolysis in terms of durability as well as efficiency.

3. Conclusions

The coupled plasma-electrolysis process can overcome the main bottleneck of CO_2 plasmolysis, i.e., the separation of oxygen from its product gas stream. Oxygen separation from a CO_2 plasmolysis equivalent mixture was achieved using a symmetrical perovskite electrode (electrolyte supported) SOEC architecture. The contribution of the three main reactions, i.e., CO oxidation, O_2 pumping, and CO_2 electrolysis, in the valorisation of the plasmolysis product stream has been analysed in over a wide temperature range. CO losses (via CO oxidation) are significant, and increase with increasing operating temperature (15–48% losses at 650–850 °C). However, under polarization, we observed that oxygen separation can be achieved (i.e. the product stream contains up to 91% less oxygen when compared to the plasmolysis one). Increasing the applied potential is a knob to turn for increased (up to 138%) CO production via CO_2 electrolysis that counterbalance CO losses. Furthermore, CO_2 plasmolysis equivalent mixture operation proved

beneficial for the durability of the process in comparison with conventional CO_2 electrolysis. Durability tests (100 h) showed that the presence of oxygen in the plasmolysis equivalent gas mixture is benign to electrode structural integrity. Our findings suggest that utilizing advanced SOEC architectures could further improve the valorisation of the CO_2 plasmolysis product stream, since high current densities can be achieved at low operating temperatures (<600 °C). Further research is needed in order to define electrode materials with lower catalytic activity for CO oxidation in order to mitigate the CO loses and advanced SOEC architectures to decrease the energy consumption for O_2 separation. Coupled plasmolysis to SOEC technology provides a promising avenue to recycling CO_2 emissions towards for CO_2 neutral chemistry and fuel production.

CRediT authorship contribution statement

MNT, AG and MvdS conceived the idea of the study. MNT and SW supervised the study. AP performed the experiments, analysed the data and wrote the manuscript. VK and DN gave input on the materials and electrochemical cells. AG, MvdS and MNT secured the funding for the project. All authors reviewed and edited the manuscript.

Declaration of Competing Interest

The authors declare that they have no known competing financial interests or personal relationships that could have appeared to influence the work reported in this paper.

Data Availability

The experimental data in this study have been deposited as excel files in the Zenodo database https://doi.org/10.5281/zenodo.5886628.

Acknowledgements

This work is part of the European project KEROGREEN, which has received funding from the European Union's Horizon 2020 Research and Innovation Programme under Grant Agreement 763909. Authors thank E. Langereis (DIFFER) for the illustrations and Cerpotech for the electrode materials.

Appendix A. Supporting information

Supplementary data associated with this article can be found in the online version at doi:10.1016/j.jcou.2022.101904.

References

[1] International energy outlook 2010, in: Int. Energy Outlook Proj., 2011.
[2] R.B. Jackson, J.G. Canadell, C. Le Quéré, R.M. Andrew, J.I. Korsbakken, G. P. Peters, N. Nakicenovic, Reaching peak emissions, Nat. Clim. Chang. 6 (2016) 7–10, https://doi.org/10.1038/nclimate2892.
[3] R.A. Verzijlbergh, L.J. De Vries, G.P.J. Dijkema, P.M. Herder, Institutional challenges caused by the integration of renewable energy sources in the European electricity sector, Renew. Sustain. Energy Rev. 75 (2017) 660–667, https://doi.org/10.1016/j.rser.2016.11.039.
[4] T.M. Gür, Review of electrical energy storage technologies, materials and systems: challenges and prospects for large-scale grid storage, Energy Environ. Sci. 11 (2018) 2696–2767, https://doi.org/10.1039/C8EE01419A.
[5] Z.J. Schiffer, K. Manthiram, Electrification and decarbonization of the chemical industry, Joule 1 (2017) 10–14, https://doi.org/10.1016/j.joule.2017.07.008.
[6] C. Chen, J.F. Khosrowabadi Kotyk, S.W. Sheehan, Progress toward commercial application of electrochemical carbon dioxide reduction, Chem 4 (2018) 2571–2586, https://doi.org/10.1016/j.chempr.2018.08.019.
[7] V. Kumaravel, J. Bartlett, S.C. Pillai, Photoelectrochemical conversion of carbon dioxide (CO_2) into fuels and value-added products, ACS Energy Lett. 5 (2020) 486–519, https://doi.org/10.1021/acsenergylett.9b02585.
[8] R. Snoeckx, A. Bogaerts, Plasma technology – a novel solution for CO_2 conversion? Chem. Soc. Rev. 46 (2017) 5805–5863, https://doi.org/10.1039/C6CS00066E.
[9] S. Jin, Z. Hao, K. Zhang, Z. Yan, J. Chen, Advances and challenges for the electrochemical reduction of CO_2 to CO: from fundamentals to industrialization, Angew. Chem. Int. Ed. 60 (2021) 20627–20648, https://doi.org/10.1002/anie.202101818.
[10] H. An, L. Wu, L.D.B. Mandemaker, S. Yang, J. Ruiter, J.H.J. Wijten, J.C.L. Janssens, T. Hartman, W. Stam, B.M. Weckhuysen, Sub-second time-resolved surface-enhanced raman spectroscopy reveals dynamic CO intermediates during electrochemical CO_2 reduction on copper, Angew. Chem. Int. Ed. 60 (2021) 16576–16584, https://doi.org/10.1002/anie.202104114.
[11] J. van de Loosdrecht, F.G. Botes, I.M. Ciobica, A. Ferreira, P. Gibson, D.J. Moodley, A.M. Saib, J.L. Visagie, C.J. Weststrate, J.W. Niemantsverdriet, Fischer–Tropsch Synthesis: Catalysts and Chemistry, in: Compr. Inorg. Chem. II, Elsevier, 2013, pp. 525–557, https://doi.org/10.1016/B978-0-08-097774-4.00729-4.
[12] R. Küngas, Review—electrochemical CO_2 reduction for CO production: comparison of low- and high-temperature electrolysis technologies, J. Electrochem. Soc. 167 (2020), 044508, https://doi.org/10.1149/1945-7111/ab7099.
[13] Y. Zheng, J. Wang, B. Yu, W. Zhang, J. Chen, J. Qiao, J. Zhang, A review of high temperature co-electrolysis of H_2O and CO_2 to produce sustainable fuels using solid oxide electrolysis cells (SOECs): advanced materials and technology, Chem. Soc. Rev. 46 (2017) 1427–1463, https://doi.org/10.1039/C6CS00403B.
[14] D. Marxer, P. Furler, M. Takacs, A. Steinfeld, Solar thermochemical splitting of CO_2 into separate streams of CO and O_2 with high selectivity, stability, conversion, and efficiency, Energy Environ. Sci. 10 (2017) 1142–1149, https://doi.org/10.1039/C6EE03776C.
[15] R.C. Pullar, R.M. Novais, A.P.F. Caetano, M.A. Barreiros, S. Abanades, F.A. C. Oliveira, A review of solar thermochemical CO_2 splitting using ceria-based ceramics with designed morphologies and microstructures, Front. Chem. 7 (2019), https://doi.org/10.3389/fchem.2019.00601.
[16] M. Schreier, F. Héroguel, L. Steier, S. Ahmad, J.S. Luterbacher, M.T. Mayer, J. Luo, M. Grätzel, Solar conversion of CO_2 to CO using Earth-abundant electrocatalysts prepared by atomic layer modification of CuO, 17087-3431, Nat. Energy 2 (2017), https://doi.org/10.1038/nenergy.2017.87.
[17] D. Yang, H. Yu, T. He, S. Zuo, X. Liu, H. Yang, B. Ni, H. Li, L. Gu, D. Wang, X. Wang, Visible-light-switched electron transfer over single porphyrin-metal atom center for highly selective electroreduction of carbon dioxide, Nat. Commun. 10 (2019) 3844, https://doi.org/10.1038/s41467-019-11817-2.
[18] C. Li, T. Wang, B. Liu, M. Chen, A. Li, G. Zhang, M. Du, H. Wang, S.F. Liu, J. Gong, Photoelectrochemical CO 2 reduction to adjustable syngas on grain-boundary-mediated a-Si/TiO 2 /Au photocathodes with low onset potentials, Energy Environ. Sci. 12 (2019) 923–928, https://doi.org/10.1039/C8EE02768D.
[19] J. Ran, M. Jaroniec, S. Qiao, Cocatalysts in semiconductor-based photocatalytic CO_2 reduction: achievements, challenges, and opportunities, Adv. Mater. 30 (2018), 1704649, https://doi.org/10.1002/adma.201704649.
[20] D. Ray, P. Chawdhury, K.V.S.S. Bhargavi, S. Thatikonda, N. Lingaiah, C. Subrahmanyam, Ni and Cu oxide supported γ-Al2O3 packed DBD plasma reactor for CO_2 activation, J. CO_2 Util. 44 (2021), 101400, https://doi.org/10.1016/j.jcou.2020.101400.
[21] Y. Qin, G. Niu, X. Wang, D. Luo, Y. Duan, Status of CO_2 conversion using microwave plasma, J. CO2 Util. 28 (2018) 283–291, https://doi.org/10.1016/j.jcou.2018.10.003.
[22] J.F. de la Fuente, A.A. Kiss, M.T. Radoiu, G.D. Stefanidis, Microwave plasma emerging technologies for chemical processes, J. Chem. Technol. Biotechnol. 92 (2017) 2495–2505, https://doi.org/10.1002/jctb.5205.
[23] G.J. van Rooij, D.C.M. van den Bekerom, N. den Harder, T. Minea, G. Berden, W. A. Bongers, R. Engeln, M.F. Graswinckel, E. Zoethout, M.C.M. van de Sanden, Taming microwave plasma to beat thermodynamics in CO_2 dissociation, Faraday Discuss. 183 (2015) 233–248, https://doi.org/10.1039/C5FD00045A.
[24] A.J. Wolf, T.W.H. Righart, F.J.J. Peeters, W.A. Bongers, M.C.M. van de Sanden, Implications of thermo-chemical instability on the contracted modes in CO 2 microwave plasmas, Plasma Sources Sci. Technol. 29 (2020), 025005, https://doi.org/10.1088/1361-6595/ab5eca.
[25] A. Goede, R. van de Sanden, CO_2-neutral fuels, Europhys. News 47 (2016) 22–26, https://doi.org/10.1051/epn/2016304.
[26] M. Alliati, D. Mei, X. Tu, Plasma activation of CO_2 in a dielectric barrier discharge: a chemical kinetic model from the microdischarge to the reactor scales, J. CO2 Util. 27 (2018) 308–319, https://doi.org/10.1016/j.jcou.2018.07.018.
[27] A. Ozkan, A. Bogaerts, F. Reniers, Routes to increase the conversion and the energy efficiency in the splitting of CO_2 by a dielectric barrier discharge, J. Phys. D Appl. Phys. 50 (2017), 084004, https://doi.org/10.1088/1361-6463/aa562c.
[28] P. Chen, J. Shen, T. Ran, T. Yang, Y. Yin, Investigation of operating parameters on CO_2 splitting by dielectric barrier discharge plasma, Plasma Sci. Technol. 19 (2017), 125505, https://doi.org/10.1088/2058-6272/aa8903.
[29] P. Ogloblina, A.S. Morillo-Candas, A.F. Silva, T. Silva, A. Tejero-del-Caz, L.L. Alves, O. Guaitella, V. Guerra, Mars in situ oxygen and propellant production by non-equilibrium plasmas, Plasma Sources Sci. Technol. 30 (2021), 065005, https://doi.org/10.1088/1361-6595/abec28.
[30] S.R. Sun, H.X. Wang, D.H. Mei, X. Tu, A. Bogaerts, CO_2 conversion in a gliding arc plasma: performance improvement based on chemical reaction modeling, J. CO2 Util. 17 (2017) 220–234, https://doi.org/10.1016/j.jcou.2016.12.009.
[31] L. Li, H. Zhang, X. Li, X. Kong, R. Xu, K. Tay, X. Tu, Plasma-assisted CO_2 conversion in a gliding arc discharge: Improving performance by optimizing the reactor design, J. CO_2 Util. 29 (2019) 296–303, https://doi.org/10.1016/j.jcou.2018.12.019.
[32] L. Li, H. Zhang, X. Li, J. Huang, X. Kong, R. Xu, X. Tu, Magnetically enhanced gliding arc discharge for CO_2 activation, J. CO2 Util. 35 (2020) 28–37, https://doi.org/10.1016/j.jcou.2019.08.021.
[33] D. Mansfeld, S. Sintsov, N. Chekmarev, A. Vodopyanov, Conversion of carbon dioxide in microwave plasma torch sustained by gyrotron radiation at frequency of

24 GHz at atmospheric pressure, J. CO2 Util. 40 (2020), 101197, https://doi.org/10.1016/j.jcou.2020.101197.
[34] L.F. Spencer, A.D. Gallimore, Efficiency of CO_2 dissociation in a radio-frequency discharge, Plasma Chem. Plasma Process 31 (2011) 79–89, https://doi.org/10.1007/s11090-010-9273-0.
[35] A. Goede, R. van de Sanden, CO_2-neutral fuels, Europhys. New 47 (2016) 22–26, https://doi.org/10.1051/epn/2016304.
[36] A. Lebouvier, S.A. Iwarere, P. D'Argenlieu, D. Ramjugernath, L. Fulcheri, Assessment of carbon dioxide dissociation as a new route for syngas production: a comparative review and potential of plasma-based technologies, Energy Fuels 27 (2013) 2712–2722, https://doi.org/10.1021/ef301991d.
[37] Y. Yin, T. Yang, Z. Li, E. Devid, D. Auerbach, A.W. Kleyn, CO_2 conversion by plasma: how to get efficient CO 2 conversion and high energy efficiency, Phys. Chem. Chem. Phys. 23 (2021) 7974–7987, https://doi.org/10.1039/D0CP05275B.
[38] V. Guerra, T. Silva, P. Ogloblina, M. Grofulović, L. Terraz, M.L. da Silva, C. D. Pintassilgo, L.L. Alves, O. Guaitella, The case for in situ resource utilisation for oxygen production on Mars by non-equilibrium plasmas, Plasma Sources Sci. Technol. 26 (2017) 11LT01, https://doi.org/10.1088/1361-6595/aa8dcc.
[39] A. Fridman, Plasma Chemistry, Cambridge University Press, Cambridge, 2008, https://doi.org/10.1017/CBO9780511546075.
[40] V.D. Rusanov, A.A. Fridman, G.V. Sholin, The physics of a chemically active plasma with nonequilibrium vibrational excitation of molecules, Sov. Phys. Uspekhi. 24 (1981) 447–474, https://doi.org/10.1070/PU1981v024n06ABEH004884.
[41] A. van de Steeg, P. Viegas, A. Silva, T. Butterworth, A. van Bavel, J. Smits, P. Diomede, M. van de Sanden, G. van Rooij, Redefining the microwave plasma-mediated CO_2 reduction efficiency limit: the role of O–CO_2 association, ACS Energy Lett. 6 (2021) 2876–2881, https://doi.org/10.1021/acsenergylett.1c01206.
[42] T. Kozák, A. Bogaerts, Evaluation of the energy efficiency of CO_2 conversion in microwave discharges using a reaction kinetics model, Plasma Sources Sci. Technol. 24 (2014), 015024, https://doi.org/10.1088/0963-0252/24/1/015024.
[43] A. Berthelot, A. Bogaerts, Pinpointing energy losses in CO_2 plasmas – effect on CO_2 conversion, J. CO2 Util. 24 (2018) 479–499, https://doi.org/10.1016/j.jcou.2018.02.011.
[44] A. Berthelot, A. Bogaerts, Modeling of CO_2 splitting in a microwave plasma: how to improve the conversion and energy efficiency, J. Phys. Chem. C. 121 (2017) 8236–8251, https://doi.org/10.1021/acs.jpcc.6b12840.
[45] J.F. de la Fuente, S.H. Moreno, A.I. Stankiewicz, G.D. Stefanidis, A new methodology for the reduction of vibrational kinetics in non-equilibrium microwave plasma: application to CO_2 dissociation, React. Chem. Eng. 1 (2016) 540–554, https://doi.org/10.1039/C6RE00044D.
[46] L.F. Spencer, A.D. Gallimore, CO_2 dissociation in an atmospheric pressure plasma/catalyst system: a study of efficiency, Plasma Sources Sci. Technol. 22 (2012), 015019, https://doi.org/10.1088/0963-0252/22/1/015019.
[47] G. Chen, V. Georgieva, T. Godfroid, R. Snyders, M.-P. Delplancke-Ogletree, Plasma assisted catalytic decomposition of CO_2, Appl. Catal. B Environ. 190 (2016) 115–124, https://doi.org/10.1016/j.apcatb.2016.03.009.
[48] J. Perez-Carbajo, I. Matito-Martos, S.R.G. Balestra, M.N. Tsampas, M.C.M. van de Sanden, J.A. Delgado, V.I. Águeda, P.J. Merkling, S. Calero, Zeolites for CO 2 –CO–O 2 separation to obtain CO 2 -neutral fuels, ACS Appl. Mater. Interfaces 10 (2018) 20512–20520, https://doi.org/10.1021/acsami.8b04507.
[49] A. Luna-Triguero, J.M. Vicent-Luna, M.J. Jansman, G. Zafeiropoulos, M. N. Tsampas, M.C.M. van de Sanden, H.N. Akse, S. Calero, Enhancing separation efficiency in European syngas industry by using zeolites, Catal. Today 362 (2021) 113–121, https://doi.org/10.1016/j.cattod.2020.03.061.
[50] A. Hauch, R. Küngas, P. Blennow, A.B. Hansen, J.B. Hansen, B.V. Mathiesen, M. B. Mogensen, Recent advances in solid oxide cell technology for electrolysis, Sci. (80-.) 370 (2020) eaba6118, https://doi.org/10.1126/science.aba6118.
[51] C. Neofytidis, E. Ioannidou, L. Sygellou, M. Kollia, D.K. Niakolas, Affecting the H_2O electrolysis process in SOECs through modification of NiO/GDC; experimental case of Au-Mo-Ni synergy, J. Catal. 373 (2019) 260–275, https://doi.org/10.1016/j.jcat.2019.04.002.
[52] A. Pandiyan, A. Uthayakumar, R. Subrayan, S.W. Cha, S.B. Krishna Moorthy, Review of solid oxide electrolysis cells: a clean energy strategy for hydrogen generation, Nanomater. Energy 8 (2019) 2–22, https://doi.org/10.1680/jnaen.18.00009.
[53] J. Sunarso, S. Baumann, J.M. Serra, W.A. Meulenberg, S. Liu, Y.S. Lin, J.C. Diniz da Costa, Mixed ionic–electronic conducting (MIEC) ceramic-based membranes for oxygen separation, J. Memb. Sci. 320 (2008) 13–41, https://doi.org/10.1016/j.memsci.2008.03.074.
[54] W.A. Meulenberg, F. Schulze-Küppers, W. Deibert, T. Van Gestel, S. Baumann, Keramische membranen: materialien – bauteile – potenzielle anwendungen, Chem. Ing. Tech. 91 (2019) 1091–1100, https://doi.org/10.1002/cite.201900019.
[55] S.S. Hashim, A.R. Mohamed, S. Bhatia, Oxygen separation from air using ceramic-based membrane technology for sustainable fuel production and power generation, Renew. Sustain. Energy Rev. 15 (2011) 1284–1293, https://doi.org/10.1016/j.rser.2010.10.002.
[56] P. Iora, P. Chiesa, High efficiency process for the production of pure oxygen based on solid oxide fuel cell–solid oxide electrolyzer technology, J. Power Sources 190 (2009) 408–416, https://doi.org/10.1016/j.jpowsour.2009.01.045.
[57] S. Gunduz, D.J. Deka, U.S. Ozkan, Advances in high-temperature electrocatalytic reduction of CO_2 and H2O, Adv. Catal. (2018) 113–165, https://doi.org/10.1016/bs.acat.2018.08.003.
[58] J.T.S. Irvine, D. Neagu, M.C. Verbraeken, C. Chatzichristodoulou, C. Graves, M. B. Mogensen, Evolution of the electrochemical interface in high-temperature fuel cells and electrolysers, Nat. Energy 1 (2016) 15014, https://doi.org/10.1038/nenergy.2015.14.
[59] V. Kyriakou, D. Neagu, G. Zafeiropoulos, R.K. Sharma, C. Tang, K. Kousi, I. S. Metcalfe, M.C.M. van de Sanden, M.N. Tsampas, Symmetrical exsolution of Rh nanoparticles in solid oxide cells for efficient syngas production from greenhouse gases, ACS Catal. 10 (2020) 1278–1288, https://doi.org/10.1021/acscatal.9b04424.
[60] V. Kyriakou, D. Neagu, E.I. Papaioannou, I.S. Metcalfe, M.C.M. van de Sanden, M. N. Tsampas, Co-electrolysis of H_2O and CO_2 on exsolved Ni nanoparticles for efficient syngas generation at controllable H_2/CO ratios, Appl. Catal. B Environ. 258 (2019), 117950, https://doi.org/10.1016/j.apcatb.2019.117950.
[61] A. Pandiyan, V. Di Palma, V. Kyriakou, W.M.M. Kessels, M. Creatore, M.C.M. Van De Sanden, M.N. Tsampas, Enhancing the electrocatalytic activity of redox stable perovskite fuel electrodes in solid oxide cells by atomic layer-deposited Pt nanoparticles, ACS Sustain. Chem. Eng. 8 (2020) 12646–12654, https://doi.org/10.1021/acssuschemeng.0c04274.
[62] Y. Yang, Y. Li, Y. Jiang, M. Zheng, T. Hong, X. Wu, C. Xia, The electrochemical performance and CO_2 reduction mechanism on strontium doped lanthanum ferrite fuel electrode in solid oxide electrolysis cell, Electrochim. Acta 284 (2018) 159–167, https://doi.org/10.1016/j.electacta.2018.07.187.
[63] L. Ye, M. Zhang, P. Huang, G. Guo, M. Hong, C. Li, J.T.S. Irvine, K. Xie, Enhancing CO_2 electrolysis through synergistic control of non-stoichiometry and doping to tune cathode surface structures, Nat. Commun. 8 (2017) 14785, https://doi.org/10.1038/ncomms14785.
[64] T. Liu, H. Liu, X. Zhang, L. Lei, Y. Zhang, Z. Yuan, F. Chen, Y. Wang, A robust solid oxide electrolyzer for highly efficient electrochemical reforming of methane and steam, J. Mater. Chem. A 7 (2019) 13550–13558, https://doi.org/10.1039/C9TA00467J.
[65] W.H. Kan, A.J. Samson, V. Thangadurai, Trends in electrode development for next generation solid oxide fuel cells, J. Mater. Chem. A. 4 (2016) 17913–17932, https://doi.org/10.1039/C6TA06757C.
[66] Y. Jiang, Y. Yang, C. Xia, H.J.M. Bouwmeester, $Sr_2Fe_{1.4}Mn_{0.1}Mo_{0.5}O_{6-\delta}$ perovskite cathode for highly efficient CO_2 electrolysis, J. Mater. Chem. A. 7 (2019) 22939–22949, https://doi.org/10.1039/C9TA07689A.
[67] Y. Li, X. Chen, Y. Yang, Y. Jiang, C. Xia, Mixed-conductor $Sr_2Fe_{1.5}Mo_{0.5}O_{6-\delta}$ as robust fuel electrode for pure CO 2 reduction in solid oxide electrolysis cell, ACS Sustain. Chem. Eng. 5 (2017) 11403–11412, https://doi.org/10.1021/acssuschemeng.7b02511.
[68] Y. Li, B. Hu, C. Xia, W.Q. Xu, J.P. Lemmon, F. Chen, A novel fuel electrode enabling direct CO_2 electrolysis with excellent and stable cell performance, J. Mater. Chem. A 5 (2017) 20833–20842, https://doi.org/10.1039/C7TA05750D.
[69] X. Peng, Y. Tian, Y. Liu, W. Wang, L. Jia, J. Pu, B. Chi, J. Li, An efficient symmetrical solid oxide electrolysis cell with LSFM-based electrodes for direct electrolysis of pure CO_2, J. CO_2 Util. 36 (2020) 18–24, https://doi.org/10.1016/j.jcou.2019.10.017.
[70] W. Wu, H. Ding, Y. Zhang, Y. Ding, P. Katiyar, P.K. Majumdar, T. He, D. Ding, 3D self-architectured steam electrode enabled efficient and durable hydrogen production in a proton-conducting solid oxide electrolysis cell at temperatures lower than 600 °C, Adv. Sci. 5 (2018), 1800360, https://doi.org/10.1002/advs.201800360.
[71] M. Kusnezoff, N. Trofimenko, M. Müller, A. Michaelis, Influence of electrode design and contacting layers on performance of electrolyte supported SOFC/SOEC single cells, Mater. (Basel) 9 (2016) 906, https://doi.org/10.3390/ma9110906.
[72] J. Rager, M. Zipperle, A. Sharma, J.L. MacManus-Driscoll, Oxygen stoichiometry in Sr_2FeMoO_6, the determination of Fe and Mo valence states, and the chemical phase diagram of SrO-Fe_3O_4-MoO_3, J. Am. Ceram. Soc. 87 (2004) 1330–1335, https://doi.org/10.1111/j.1151-2916.2004.tb07730.x.
[73] X. Xi, Z.-S. Cao, X.-Q. Shen, Y. Lu, J. Li, J.-L. Luo, X.-Z. Fu, In situ embedding of CoFe nanocatalysts into Sr3FeMoO7 matrix as high-performance anode materials for solid oxide fuel cells, J. Power Sources 459 (2020), 228071, https://doi.org/10.1016/j.jpowsour.2020.228071.
[74] S.R. Bishop, D. Marrocchelli, C. Chatzichristodoulou, N.H. Perry, M.B. Mogensen, H.L. Tuller, E.D. Wachsman, Chemical expansion: implications for electrochemical energy storage and conversion devices, Annu. Rev. Mater. Res. 44 (2014) 205–239, https://doi.org/10.1146/annurev-matsci-070813-113329.
[75] D. Neagu, J.T.S. Irvine, Structure and properties of $La_{0.4}Sr_{0.4}TiO_3$ ceramics for use as anode materials in solid oxide fuel cells, Chem. Mater. 22 (2010) 5042–5053, https://doi.org/10.1021/cm101508w.
[76] Y. Li, S. Zou, J. Ju, C. Xia, Characteristics of nano-structured SFM infiltrated onto YSZ backbone for symmetrical and reversible solid oxide cells, Solid State Ion. 319 (2018) 98–104, https://doi.org/10.1016/j.ssi.2018.02.003.
[77] G. Xiao, Q. Liu, F. Zhao, L. Zhang, C. Xia, F. Chen, Sr2Fe1.5Mo0.5O6 as cathodes for intermediate-temperature solid oxide fuel cells with La0.8Sr0.2Ga0.87Mg0.13O3 electrolyte, J. Electrochem. Soc. 158 (2011) B455, https://doi.org/10.1149/1.3556085.
[78] C. Graves, S.D. Ebbesen, M. Mogensen, K.S. Lackner, Sustainable hydrocarbon fuels by recycling CO_2 and H_2O with renewable or nuclear energy, Renew. Sustain. Energy Rev. 15 (2011) 1–23, https://doi.org/10.1016/j.rser.2010.07.014.
[79] M.A. Buccheri, A. Singh, J.M. Hill, Anode- versus electrolyte-supported Ni-YSZ/YSZ/Pt SOFCs: effect of cell design on OCV, performance and carbon formation for the direct utilization of dry methane, J. Power Sources 196 (2011) 968–976, https://doi.org/10.1016/j.jpowsour.2010.08.073.
[80] B.-K. Park, S.A. Barnett, Boosting solid oxide fuel cell performance via electrolyte thickness reduction and cathode infiltration, J. Mater. Chem. A 8 (2020) 11626–11631, https://doi.org/10.1039/D0TA04280C.

[81] N. Droushiotis, F.D. Grande, M.H. Dzarfan Othman, K. Kanawka, U. Doraswami, I. S. Metcalfe, K. Li, G. Kelsall, Comparison between anode-supported and electrolyte-supported Ni-CGO-LSCF micro-tubular solid oxide fuel cells, Fuel Cells 14 (2014) 200–211, https://doi.org/10.1002/fuce.201300024.
[82] D. Udomsilp, C. Lenser, O. Guillon, N.H. Menzler, Performance benchmark of planar solid oxide cells based on material development and designs, Energy Technol. 9 (2021), 2001062, https://doi.org/10.1002/ente.202001062.
[83] A. Mahmood, S. Bano, J.H. Yu, K.-H. Lee, Performance evaluation of SOEC for CO_2/H_2O co-electrolysis: considering the effect of cathode thickness, J. CO2 Util. 33 (2019) 114–120, https://doi.org/10.1016/j.jcou.2019.05.014.
[84] W. Yu, Y. Lim, S. Lee, A. Pandiyan, G.Y. Cho, S.W. Cha, Low-temperature, high-performance thin-film solid oxide fuel cells with tailored nano-column structures of a sputtered Ni anode, J. Mater. Chem. A 8 (44) (2020) 21668–21679, https://doi.org/10.1039/d0ta06255c.